SCIENTIFIC REPORTS
nature research

OPEN

Dodecin as carrier protein for immunizations and bioengineering applications

Florian Bourdeaux[1], Yannick Kopp[2], Julia Lautenschläger[1], Ines Gößner[1], Hüseyin Besir[3,5], R. Martin Vabulas[4] & Martin Grininger[1]✉

In bioengineering, scaffold proteins have been increasingly used to recruit molecules to parts of a cell, or to enhance the efficacy of biosynthetic or signalling pathways. For example, scaffolds can be used to make weak or non-immunogenic small molecules immunogenic by attaching them to the scaffold, in this role called carrier. Here, we present the dodecin from *Mycobacterium tuberculosis* (*mt*Dod) as a new scaffold protein. *Mt*Dod is a homododecameric complex of spherical shape, high stability and robust assembly, which allows the attachment of cargo at its surface. We show that *mt*Dod, either directly loaded with cargo or equipped with domains for non-covalent and covalent loading of cargo, can be produced recombinantly in high quantity and quality in *Escherichia coli*. Fusions of *mt*Dod with proteins of up to four times the size of *mt*Dod, e.g. with monomeric superfolder green fluorescent protein creating a 437 kDa large dodecamer, were successfully purified, showing *mt*Dod's ability to function as recruitment hub. Further, *mt*Dod equipped with SYNZIP and SpyCatcher domains for post-translational recruitment of cargo was prepared of which the *mt*Dod/SpyCatcher system proved to be particularly useful. In a case study, we finally show that *mt*Dod-peptide fusions allow producing antibodies against human heat shock proteins and the C-terminus of heat shock cognate 70 interacting protein (CHIP).

Abbreviations

ACP	Acyl carrier protein
AB	Antibody
BSA	Bovine serum albumin
Catcher	small protein fold (SpyCatcher or SnoopCatcher) that binds and reacts with Tag
CellSig.	Cell Signaling Technology
CHIP	C-terminus of heat shock cognate 70 interacting protein
EU	Endotoxin units
FMN	Riboflavin-5′-phosphate
GFP	Green fluorescent protein
GSG, PAS, PAS2 GPAS, GPAS2, PASG, PAS2G, linker systems	See Table 1
HB-EGF	Proheparin-binding EGF-like growth factor
HSP	Heat shock protein
IPTG	Isopropyl-β-D-thiogalactopyranoside
KLH	Keyhole limpet hemocyanin
L	Ladder (only used in figures)

[1]Institute of Organic Chemistry and Chemical Biology, Buchmann Institute for Molecular Life Sciences, Cluster of Excellence for Macromolecular Complexes, Goethe University Frankfurt, Max-von-Laue-Str. 15, 60438 Frankfurt am Main, Germany. [2]Institute of Biophysical Chemistry, Buchmann Institute for Molecular Life Sciences, Goethe University Frankfurt, Max-von-Lauer Str. 15, 60438 Frankfurt am Main, Germany. [3]European Molecular Biology Laboratory, 69117 Heidelberg, Germany. [4]Institute of Biochemistry, Charité - Universitätsmedizin Berlin, Charitéplatz 1, 10117 Berlin, Germany. [5]Present address: PROGEN Biotechnik GmbH, 69123 Heidelberg, Germany. ✉email: grininger@chemie.uni-frankfurt.de

LAL	*Limulus* amebocyte lysate
Lys	Lysate (only used in figures)
MAP	Multiple antigen peptides
*mm*ACP	*Mus musculus* acyl carrier protein
msfGFP	Monomeric superfolder green fluorescent protein
*mt*Dod	*Mycobacterium tuberculosis* dodecin
*mt*Dod(WT)	*Mycobacterium tuberculosis* dodecin wild type
OD600	Optical density at 600 nm
OE	Over expressing cells
RSA	Rabbit serum albumin
SCBT	Santa Cruz Biotechnology
*se*ACP	*Saccharopolyspora erythraea* acyl carrier protein
SEC	Size exclusion chromatography
Sfp	4′-Phosphopantetheine transferase from *Bacillus subtilis*
Sigma	Sigma-Aldrich
SnpC	SnoopCatcher
SnpT	SnoopTag
SpyC	SpyCatcher
SpyT	SpyTag
SZ	SYNZIP domain
Tag	Small peptide sequence that interacts with Catcher's (SpyTag or SnoopTag)
TB	Terrific broth
TBS	Tris-HCl buffered saline
TBST	Tris-HCl buffered saline with Tween-20
TT	Tetanus toxoid
VLP	Virus-like particle

For being suited as scaffolds, proteins need to meet an array of requirements. Depending on the actual use, multiple features of the protein can be important; e.g., particle size, achievable purity, expression level, robustness of fold/assembly, general stability and immunogenicity (if used for immunizations). Two key features are obligatory, in addition. Scaffolds need to form a stable and water-soluble structure that is best insensitive to the attached cargo, and they should further allow the dense packing of the cargo in homovalent and ideally also in heterovalent fashion[1–5].

One application of scaffold proteins is their conjugation with peptides for the generation of antibodies (AB), utilizing the increased immunogenicity of the protein-peptide conjugate (in this role often called carrier proteins)[6]. Such ABs can be used to identify proteins, which contain the peptides used for AB generation, in complex samples, and allow the specific labelling of proteins of interest in their spatiotemporal distribution, e.g. by immunofluorescence imaging or western blotting. For the reactivity of the ABs, the selection of the peptide is critical, since the ABs derived from the conjugate can only recognize the peptide as presented (or similar) on the carrier[7]. For the recognition of the protein in its native form, the correct sequence, but also the structure and surface exposure of the selected peptide need to be considered[7]. For B-cell activation, the conjugated peptide needs to be exposed on the surface of the carrier, and it is thought that a dense packing of the conjugated peptide is advantageous for this, because highly repetitive epitopes on the particle/carrier surface facilitate B-cell receptor oligomerization[1,2].

Usually peptide-carrier conjugates for AB production are formed by coupling an about 20 amino acid-long peptide to residues at the surface of a carrier protein via a chemical reaction[8–10]. Commonly used carrier proteins are keyhole limpet hemocyanin (KLH), bovine serum albumin (BSA) and rabbit serum albumin (RSA), but also other proteins, e.g. tetanus toxoid (TT), and artificial carrier-systems, e.g. multiple antigen peptides (MAP) or virus-like particles (VLP, not limited to chemical conjugations), are used[11,12]. While BSA bears typical carrier properties (likely also other albumins), and exposes the peptides at the surface at a potentially high density[13,14], KLH is often preferred as a carrier-protein due to its high immunogenicity[15,16]. Notably, the immune system reacts to the entire conjugate, and, therefore, ABs are not just raised against the peptide of interest, but also against the carrier protein and the linker (peptide or remnant of the coupling agent/crosslinker). To avoid cross-reactivity by anti-carrier or anti-linker ABs, it is beneficial to use carrier-linker systems for immunization that have no or only very low similarity with the inventory of cells and tissues that are supposed to be analysed[16].

Although the method of chemically coupling peptides of interest to carrier proteins is commonly used, it is not without weaknesses. Besides limitations arising from solid support synthesis of the peptide themselves, e.g. limited solubility of hydrophobic sequences or amyloid forming sequences, the spectrum of peptides that can be coupled to the above listed carrier proteins is constrained by its compatible with the coupling agent. For example, internal cysteine residues are avoided, because they are commonly terminally introduced for the coupling to the carrier protein[8–10]. Further, in some cases, the stability of the conjugation product or intermediate (activated carrier) can be problematic[10,17]. An alternative method to the coupling approach is the direct expression of self-assembling peptide-carrier conjugates, provided as encoding DNA sequence to the recombinant expression host. This approach allows more flexibility in the design of epitopes and linkers, since the limitations of coupling reactions or peptide synthesis need not be taken into account. Self-assembling carrier proteins can also be produced with tags or proteins that allow post-translational covalent linking of cargo, thereby not relying

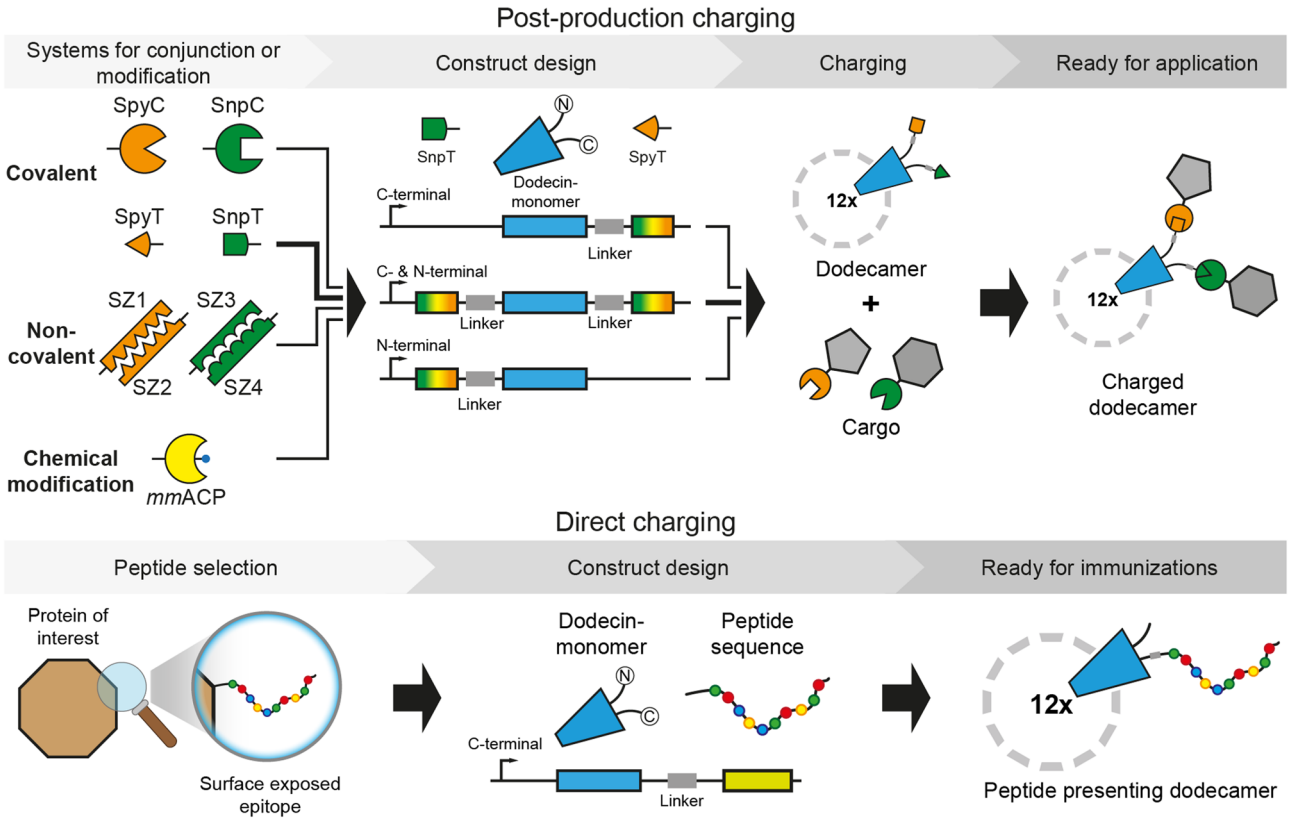

Figure 1. Schematic depiction of *mt*Dod constructs and workflow presented in this study. In this study, termini were modified directly at gene level with peptides, domains or proteins for subsequent charging with cargo (top) or direct coupling of peptides for immunizations (bottom). The dodecamers expose their termini at the outer surface. (Top) Selected example is highlighted by arrows in bold. SpyT and SpyC: SypTag and SpyCatcher[25,26]. SnpT and SnpC: SnoopTag and SnoopCatcher[27]. SZ1-SZ4: helical domains that bind to their specific counterpart, called SYNZIP[28]. *Mm*ACP: *Mus musculus* acyl carrier protein (ACP), gene *Fasn*.

on chemical coupling[18,19]. While this carrier method has high potential, it is reliant on the availability of stable and robust self-assembling protein- and peptide-scaffolds.

The dodecin protein family was recently discovered as a flavin storage and buffering system that occurs in bacteria and archaea, but not in eukaryotes[20–23]. Dodecins are 8 kDa small proteins of βαββ-topology. Although forming a small antiparallel β-sheet that partly enwraps the helix, the dodecin fold is unique. Dodecins largely meet the requirements of protein scaffolds. In the native dodecameric state, dodecins are of spherical shape with 23-cubic symmetry, and the N- and C-termini are exposed at the protein surface. Dodecins show pronounced thermostability (> 95 °C)[22–24], which likely originates from an extensive antiparallel β-sheet that is built upon protomer assembly.

Here, we present dodecin from *Mycobacterium tuberculosis* (*mt*Dod) as a new carrier protein for peptides and scaffold for bioengineering applications. To evaluate *mt*Dod's suitability as a carrier/scaffold protein, we expressed and purified diverse *mt*Dod fusion constructs, and analysed the obtained dodecamers. The robustness of the dodecamer assembly was probed by the ability to express the diverse constructs as dodecamers in *Escherichia coli*. Further, we analysed the stability of the obtained dodecamers, and found that it is largely unaffected by the attached tag, linker and/or cargo. Finally, we demonstrate that the use of *mt*Dod as a carrier benefits from its accessibility in high amounts via by a simple heat denaturation protocol. *Mt*Dod conjugates with heat sensitive cargo were purified via conventional affinity chromatography.

The exposed termini of *mt*Dod can be harnessed for charging/functionalization in diverse ways of which we used two in this study: First, a cargo was directly fused by attaching the peptide/protein-encoding sequence at the gene level. Second, *mt*Dod was terminally modified with conjugation sites that allow post-translational covalent and non-covalent fusions of the peptide/protein as well as other chemical entities to the intact dodecin carrier (Fig. 1). In a case study, we directly tested the suitability of *mt*Dod as carrier for producing anti-peptide ABs for laboratory use. ABs were raised in rabbits against *mt*Dod-peptide fusions, and showed comparable labelling capability as commercially available ABs judged by western blotting.

Results and discussion

Dodecin can be recombinantly produced in high yields. To evaluate the suitability of *mt*Dod as a carrier protein, several *mt*Dod constructs were designed and purified. All constructs were expressed in *E. coli* BL21 (DE3). Cells were grown in terrific broth (TB) medium to an optical density at 600 nm (OD_{600}) of about

Construct name	Linker system	Molar mass/Da	Expression state[#]
mtDod-peptides			
*mt*Dod(WT)	–	7,497	Soluble
*mt*Dod-GSG-Lys	GSG	8,411	Soluble
*mt*Dod-PAS-Met	PAS	8,876	Soluble
*mt*Dod-SpyT	PASG	10,458	Soluble
SpyT-*mt*Dod	GPAS	10,215	Soluble
*mt*Dod-PAS2-SpyT	PAS2G	11,447	Soluble
SpyT-PAS2-*mt*Dod	GPAS2	11,205	Soluble
SpyT-*mt*Dod-SnpT	GPAS / PASG	13,142	Soluble
mtDod-proteins			
*mt*Dod-*mm*ACP	PAS	17,994	Soluble
*mt*Dod-*mm*ACP-H8	PAS	19,334	Soluble
*mt*Dod-msfGFP-H8	PAS	36,388	Soluble
*mt*Dod-SpyC-H8*	PAS	22,413	Inclusion body
H8-SpyC-*mt*Dod	PAS	22,072	Inclusion body
*mt*Dod-SZ1**	PAS	14,232	Inclusion body
*mt*Dod-SZ3**	PAS	13,396	Inclusion body
*mt*Dod-*se*ACP***	PAS	19,966	Inclusion body

Linker details			
GSG:	GGGGSGGGG	PAS:	SPAAPAPASPAS
PASG:	SPAAPAPASPASGGSG	GPAS:	GGSGSPAAPAPASPAS
PAS2G:	SPAAPAPASPASPAPSAPAASPAAGGSG	GPAS2:	GGSGSPAAPAPASPASPAPSAPAAS-PAA

Table 1. Selection of *mt*Dod constructs used for expression studies are divided into two groups: *mt*Dod-peptides (constructs with only short peptides fused to *mt*Dod) and *mt*Dod-proteins (constructs with domains or entire proteins fused to *mt*Dod). *mt*Dod(WT): wild type *mt*Dod. *se*ACP: *Saccharopolyspora erythraea* ACP, gene *chlB2*. msfGFP: monomeric superfolder green fluorescent protein[29]. For a full description of constructs, see Supplementary Table S1. The constructs *mt*Dod-GSG-Lys and *mt*Dod-PAS-Met have been used as control; *Mt*Dod-GSG-Lys was used for its flexible linker, and *mt*Dod-PAS-Met for its rigid linker. The PAS linker were based on sequences (slight alterations) shown in ref[30]. [#]Describes whether the major fraction of the expressed construct is soluble or forms inclusion bodies. *Mt*Dod constructs with low solubility form often non-classical inclusion bodies (correctly folded protein)[31], leading to their yellowish colouring (flavin binding). Since flavin binding only requires intact *mt*Dod, it is possible that inclusion bodies are yellow although the protein cargo is misfolded. **Mt*Dod-SpyC-H8 seems to be soluble in cellular environment but forms yellow aggregates after cell lysis. **SZ1-*mt*Dod and SZ3-*mt*Dod also formed inclusion bodies and behaved similarly as the C-terminal constructs (data not shown). ***Mt*Dod-*se*ACP could not be obtained in soluble form; under all applied refolding conditions yellow aggregate was formed.

0.6–0.8 at 37 °C before induction with isopropyl-β-D-thiogalactopyranoside (IPTG; 0.5 mM final concentration), and expression was performed over night at 20 °C. Since *mt*Dod is a flavin binding protein (preferred flavin-ligand is riboflavin-5′-phosphate (FMN))[23,24], its overexpression causes increased amounts of cellular flavin, leading to a yellowish colouring of the cells. Cells were lysed by French press, and the cell debris was removed by centrifugation. Depending on the *mt*Dod construct different purification strategies were applied. In the following, construct names are underlying the nomenclature: peptides or proteins fused to the N-terminus of a protein are written in front of the protein (e.g. peptide-*mt*Dod) and C-terminal fusions are written after the protein (e.g. *mt*Dod-peptide). Most *mt*Dod constructs were produced as soluble proteins, but some proteins, such as *mt*Dod-SZ1, *mt*Dod-SZ3 (SYNZIP constructs)[28], H8-SpyC-*mt*Dod and *mt*Dod-SpyC-H8 (SpyC constructs)[25,26] accumulated as inclusion bodies (Table 1).

For soluble *mt*Dod constructs, most cytosolic *E. coli* proteins were removed by heat denaturation at about 75 °C. *Mt*Dod itself is stable to temperatures above 95 °C under standard conditions (pH ~ 7.5 and ionic strength > 100 mM, e.g., in PBS), and the thermal stability can be further increased by adding the native FMN ligand in excess[23,24]. Depending on the stability of the fused cargo, lower temperatures during the heat denaturation may be necessary, or different purification approaches need to be applied (affinity chromatography). For example, *mt*Dod-*mm*ACP started to precipitate at about 55–60 °C in spite of *mt*Dod staying intact, as indicated by maintained FMN binding and preserved dodecameric stability (Supplementary Fig. S1). In this case, heat denaturation was conducted at about 55 °C. Lower temperatures during the heat denaturation step can affect the purity of preparations, because some *E. coli* proteins remain soluble. Following heat treatment, *mt*Dod constructs were generally further purified by two cycles of DMSO-induced precipitation (50% final DMSO concentration). Finally, size-exclusion chromatography (SEC) was performed to select for dodecameric fractions, which can be

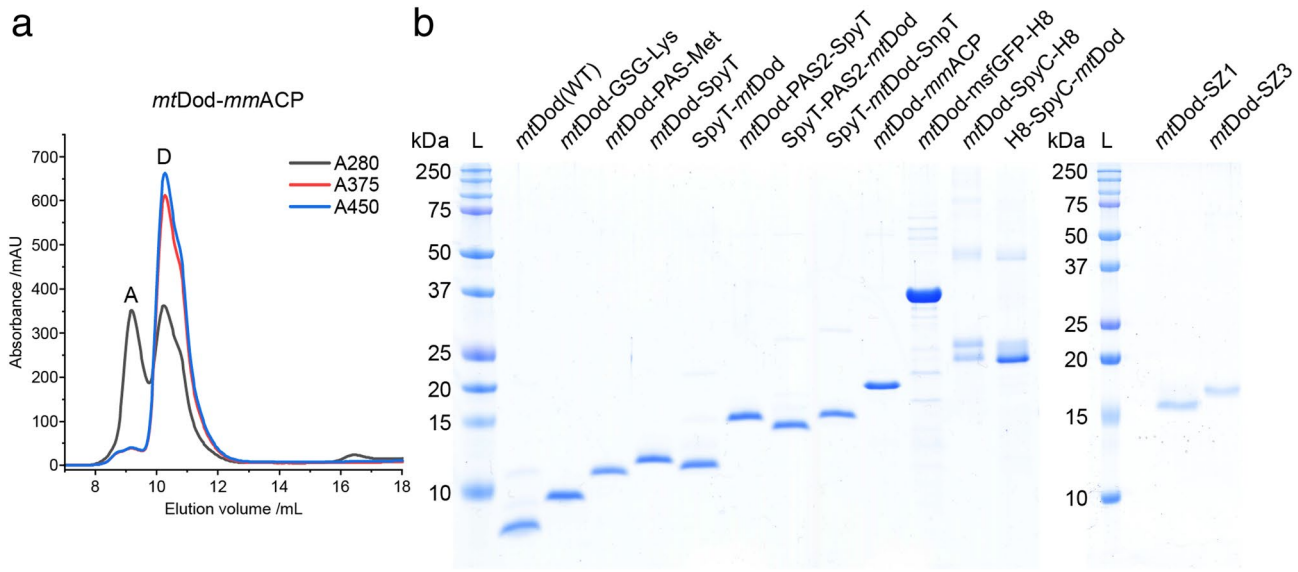

Figure 2. SEC profile of *mt*Dod-*mm*ACP and SDS-PAGE gel of various *mt*Dod constructs. (**a**) SEC chromatogram of *mt*Dod-*mm*ACP after heat denaturation and DMSO precipitation. Used column: Superdex 200 increase 10/300 column (GE Healthcare). A: peak representing aggregates. D: peak representing the dodecamer. The oligomerization status was assigned based on the absorption at 375 nm (A375) and 450 nm (A450) (indicating bound flavin) and their elution volume (species at lowest molecular weight eluting with bound flavin). Although *mt*Dod-*mm*ACP in general formed yellow coloured aggregates, the here observed aggregate does not show flavin absorption bands, indicating that this aggregate does not contain dodecameric species. (**b**) SDS-PAGE gel of purified *mt*Dod constructs. L: Ladder. For full dissociation of the dodecamers in SDS-PAGE, an acidic loading buffer containing 3.3% SDS was used during the heat treatment (5 min 60 °C). After the heat treatment, the pH was increased to about 6.8 using a glycerol- and Tris–HCl-containing buffer, followed by a second heat treatment (5 min 95 °C). *Mt*Dod-SZ1 and *mt*Dod-SZ2 were denatured with loading buffer containing ~7 M urea and 2.5% SDS (prolonged heat treatment: 15 min 95 °C). Denaturation with acidic loading buffer was more reliable for most constructs and easier in handling compared to urea-based protocols (in some cases even 7–8 M urea failed to dissociate the protein completely). Of note, when treated with acidic loading buffer, some constructs showed additional bands (mainly SpyC constructs, Supplementary Fig. S5). The origin of this behaviour was not further investigated.

easily identified by the absorption bands of bound flavin (375 nm and 450 nm). For *mt*Dod-peptide fusions, the dodecamer turned out to be the main oligomeric species. While only minor peaks representing lower oligomeric states were detected, aggregation peaks were observed at high concentrations (Supplementary Fig. S2). For larger *mt*Dod constructs with fused proteins, like *mt*Dod-*mm*ACP (Fig. 2a), significant aggregation was observed in the SEC profiles (see Supplementary Fig. S2).

For the construct *mt*Dod-msfGFP-H8, purification by heat denaturation (70 °C, above that aggregation was observed) and purification by affinity chromatography were compared. GFP is a suitable cargo for this test, because GFP is highly thermostable[32]. The dodecameric structure of dodecin causes a high density of surface exposed affinity tags, allowing vigorous washing without severe protein loss during Ni-chelating affinity chromatography. Accordingly, *mt*Dod-msfGFP-H8 was washed with two column volumes of a 200 mM imidazole-containing wash buffer, and elution was performed at 400 mM imidazole. While with both purification strategies *mt*Dod-msfGFP-H8 dodecamer was obtained, the sample purified by heat denaturation showed severe aggregation in SEC (Supplementary Fig. S3).

*Mt*Dod constructs that aggregate in inclusion bodies can be refolded by dialysis, as previously described[23], under conditions optimized for the respective fused cargo. All inclusion bodies were first washed and then dissolved by denaturation using 6 M guanidinium chloride. *Mt*Dod was refolded without further purification at different conditions ranging from pH 5.0[23] to pH 8.5. Refolding was possible for all constructs obtained as inclusion bodies in this study, although the resolubilized proteins remained aggregation-prone, particularly during protein concentration and filtration. For a screen of buffer conditions for refolding constructs *mt*Dod-SpyC-H8 and H8-SpyC-*mt*Dod, see Supplementary Fig. S4. Notably, for both constructs, a glycerol-containing buffer was found to be best suited for refolding.

Overall, all constructs presented in Table 1, except *mt*Dod-*se*ACP, were obtained in high purity (see Fig. 2b).

We thought that the insolubility and aggregation problems observed for some constructs may be solved by the formation of *mt*Dod-heterododecamers, because then the density of entities on the surface could be reduced. To probe heterododecamer formation with *mt*Dod in vitro and in vivo, we worked with the two species *mt*Dod-PAS-Strep and *mt*Dod(WT). We note that *mt*Dod-PAS-Strep was used for its availability in the lab and is not compromised in solubility. We assume that other *mt*Dod-PAS-peptide constructs than *mt*Dod-PAS-Strep could have been used, too. For in vitro heterododecamer formation, *mt*Dod(WT) and *mt*Dod-PAS-Strep were jointly refolded in different relative concentrations, while for the formation of heterododecamers in vivo,

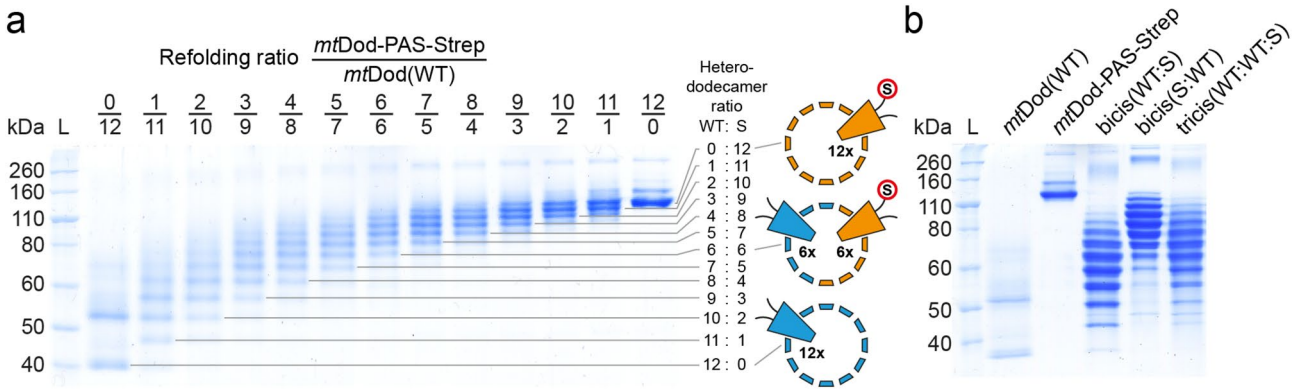

Figure 3. SDS-PAGE gel of purified heterododecamers of *mt*Dod(WT) (WT, light blue in cartoon) and *mt*Dod-PAS-Strep (S, orange with red encircled "S"). L: Ladder. For analysis of heterododecamer composition, the Tris–glycine (Lämmli) SDS-PAGE system was used, and samples were prepared without heat treatment and SDS (for full length gel images see Supplementary Fig. S6). For *mt*Dod(WT) two bands at about 40 kDa and slightly above 50 kDa are observable (both below the weight of the dodecamer, about 90 kDa). The band at about 40 kDa represents likely the dodecamer and the band above seems to be caused by the mild denaturation conditions during sample preparation. The appearance of additional bands at higher molecular weight is also observable in other lanes. We want to note that these bands don't depict the hexamer and the dodecamer, as all protein–protein interactions, which would stabilize the hexamer, are present in higher numbers in the dodecamer with also other additional stabilizing interactions. The origin of the *mt*Dod dodecamer migration behaviour and the molecular mechanism behind the bands at higher molecular weight is not clear. (**a**) SDS-PAGE gel of heterododecamers obtained by refolding *mt*Dod(WT) and *mt*Dod-PAS-Strep at different ratios. Each band represents a heterododecamer with a defined composition of *mt*Dod-PAS-Strep and *mt*Dod(WT) (13 bands for 13 possible compositions, higher molecular weight bands above about 160 kDa excluded). (**b**) SDS-PAGE gel of purified heterododecamers formed during polycistronic expression of *mt*Dod(WT) and *mt*Dod-PAS-Strep. Bicis(WT:S): Bicistronic expression vector design: *mt*Dod(WT) encoding gene first and *mt*Dod-PAS-Strep encoding gene second. Bicis(S:WT): Bicistronic expression vector design: *mt*Dod-PAS-Strep encoding gene first and *mt*Dod(WT) encoding gene second. Tricis(WT:WT:S): Tricistronic expression vector design: *mt*Dod(WT) encoding gene first and second and *mt*Dod-PAS-Strep encoding gene third.

three combinations of the *mt*Dod constructs were expressed polycistronically. The analysis of heterododecamer compositions was possible by the high stability of the dodecamers (see Supplementary Fig. S5 for *mt*Dod(WT) dodecamer observable in SDS-PAGE) and the different migration behaviour of constructs/species in SDS-PAGE (Fig. 3). The slower migration of *mt*Dod-PAS-Strep is likely caused by the limited binding of SDS to the exposed PAS sequence (see Fig. 2b *mt*Dod-GSG-Lys compared to *mt*Dod-PAS-Met)[30]. Data indicates that the composition of heterododecamers is controlled by the relative concentration of species in the refolding solution,i.e., the higher the concentration of a construct, the more abundant it is in the refolded dodecamer. Of note, assuming that the heterododecamer formation is just controlled by the concentration of each construct (see Fig. 3a), the band patterns for heterododecamers assembled in vivo can be used to estimate gene order related expression strength (see Fig. 3b), as described in the literature for other methods, e.g. FRET[33]. The estimated relative expression strength of each gene is for the bicistronic vector: first > second, and for the tricistronic vector first > third > second.

Dodecin is highly stable. We have recently established the cyclic thermal shift assay, termed thermocyclic fluorescence assay, to determine the stability of dodecins[23]. This assay is based on the fluorescence quenching that is observed when flavins bind to dodecin. In each binding pocket of the dodecamer, the two isoalloxazine ring systems of two bound flavins are embedded between symmetry-related tryptophans.[22–34] Since dodecins can only bind flavins in the dodecameric state, the fluorescence intensity of flavins can be used to estimate the amount of dodecameric *mt*Dod in solution. In contrast to standard melting analysis, in which the temperature is continuously increased, the thermocyclic fluorescence assay runs cyclic temperature profiles that contain a heating phase (temperature increased per cycle) and a cooling phase (for all cycles cooled to 5 °C). At the heating phase, FMN is released from the binding pocket and the fluorescence intensity increases. During cooling, FMN can rebind to the dodecamer (cooling phase) restoring initial low fluorescence values. As soon as the dodecamer denatures irreversibly, the fluorescence intensity remains at elevated levels. By plotting the fluorescence intensity of the cooling phase against the heating phase temperature, the thermal stability of the dodecamer of the *mt*Dod constructs can be determined.

Since all constructs, except *mt*Dod-SZ1 and *mt*Dod-SpyC-H8, proved to be stable in PBS buffer throughout the entire temperature range, we identified the slightly destabilizing conditions of pH 4.2 as suited to sense the impact of the cargo on the integrity of the *mt*Dod dodecameric scaffold (see Fig. 4). Under this condition, the thermally stable constructs *mt*Dod(WT) and *mt*Dod-peptides started to denature at 75–80 °C. Of note, we considered a protein to denature when the fluorescence curve reached its knee right before going into a steep increase in fluorescence reaching values of above 30%. It is further important to note that the thermocyclic fluorescence assay does only monitor the dodecameric stability, which may be influenced by the attached cargo. For

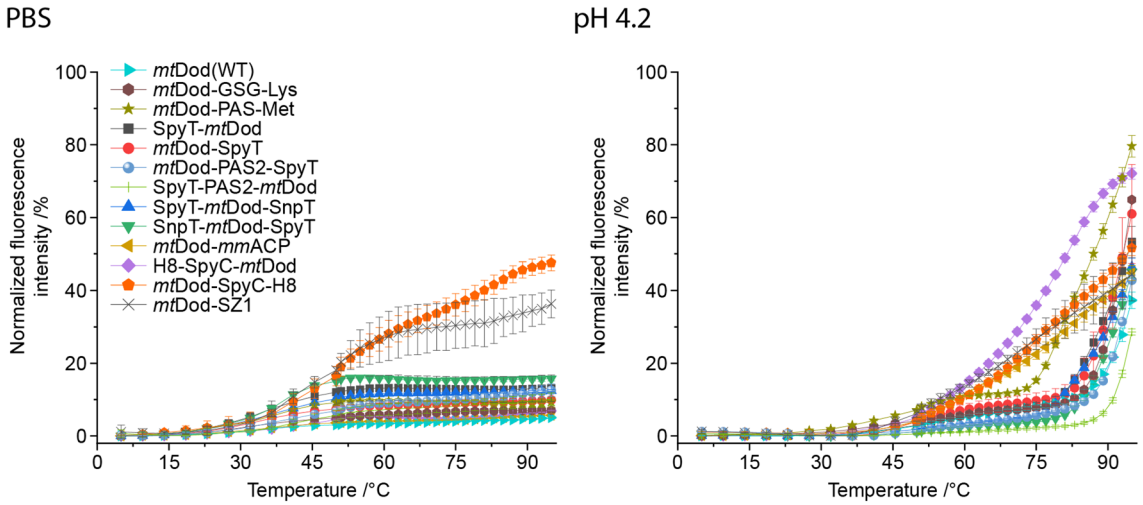

Figure 4. Thermal stablity of *mt*Dod constructs. The FMN fluorescence at the rebinding/cooling phase is plotted against the heating phase temperature. The increase of FMN fluorescence indicates disassembly of the dodecamer at the heating phase, as the flavin cannot rebind in the cooling phase and its fluorescence is not quenched. In PBS, only a negligible increase of fluorescene is observed within the entire temperature range, except for *mt*Dod-SpyC and *mt*Dod-SZ1, indicating that the dodecameric *mt*Dod core structures do not disassemble. The minor increase of fluorescence of up to 20% around 45–50 °C might be caused by hindered rebinding of FMN and not by disassembling of the dodecamer. At pH 4.2, for all constructs, a steep (compared to PBS data) increase of fluorescence is observable indicating the dodecamer disassambly. Most constructs behave like *mt*Dod(WT), and are stable to about 80 °C, except *mt*Dod-PAS-Met, *mt*Dod-*mm*ACP, *mt*Dod-SpyC-H8 and H8-SpyC-*mt*Dod of which the latter three start denaturing already at 50 °C. *mt*Dod-PAS-Met is only slightly less stable, and starts to denature around 75 °C. Note that *mt*Dod-SpyC-H8 and *mt*Dod-SZ1 suffer from strongly impaired FMN binding leading to non-saturated binding sites, and data needs to be treated with care. The FMN binding may also be altered by denaturing/aggregation of the fused fold, causing different curve profiles, e.g. *mt*Dod-*mm*ACP. For all measurements, fluorescence was normalized to the maximum values recorded in the heating phase, corrected by the temperature-induced fluorescence decline of FMN. Curves connect the averages of three technical replicates. Standard deviations are shown as error bars.

example, in screening temperatures for the heat denaturation of *mt*Dod-*mm*ACP, we observed the formation of yellowish agglomerates above 55–60 °C, indicating that the construct is intact in the *mt*Dod scaffold, as capable of FMN binding, but precipitated by the thermally unfolded *mm*ACP (band representing the intact dodecamer observable in SDS PAGE, see Supplementary Fig. S7).

The high dodecameric stability of *mt*Dod is also observed in SDS-PAGE using the standard loading buffer (2.5% SDS, pH 6.8) (see Supplementary Fig. S5). Under these conditions, further depending on the heat treatment for sample preparation, a dodecameric fraction remains intact, as indicated by the high molecular weight band representing the dodecamer. In accordance to the lower stability at pH 4.2, observed in the thermocyclic fluorescence assay, a two-component acidic loading buffer (3.3% SDS and pH < 4.2 during heat treatment, afterwards 2.5% SDS and pH 6.8) was applied to fully denature the dodecamer (Fig. 2).

While we did not study the effects of freezing and thawing explicitly, we would like to note that we did not observe noticeable aggregation for most *mt*Dod constructs after freezing and thawing (all constructs presented here were frozen and thawed at least once). However, constructs that are prone to aggregation might be problematic during freezing and thawing. Accordingly, we noticed aggregation for *mt*Dod-msfGFP-H8, indicated by green fluorescent aggregates after thawing, and *mt*Dod SYNZIP constructs, forming yellowish precipitate. For SpyC *mt*Dod constructs, glycerol containing buffer could prevent noticeable aggregation after freezing and thawing.

Peptides/proteins fused to *mt*Dod remain functional. The accessibility and functionality of folds and peptides fused to *mt*Dod were tested by the reactivity of the SpyT/-C and SnpT/-C pairs[25–27]. These systems allow the covalent conjugation between two entities of which one is equipped with a peptide tag (Tag) and the other with a small protein fold (Catcher)[26]. Applications range from attaching proteins from pathogens to scaffolds, like VLPs and IMX313 (heptamer forming coiled coils), for immunizations[18,19], to recruiting enzymes to a scaffold hub for creating assemblies with elevated substrate turnover[35]. In this study, *se*ACP-SpyC and mClover3-SnpC were prepared as cargo for performing SpyT/-C and SnpT/-C reactions with the respective Tag-labelled *mt*Dod constructs. For the inverse reaction, *mt*Dod SpyC constructs and SpyT-*se*ACP were used. For all reactions, the scaffold was saturated with two molar equivalents of cargo. The reactions were incubated for 20 h at 22 °C, and analysed by SDS-PAGE (Fig. 5).

For all combinations of *mt*Dod scaffold and cargo, the expected product band(s) of *mt*Dod and the specific cargo(s) were observed in SDS-PAGE. While for *mt*Dod SpyT/SnpT constructs no unreacted scaffold proteins was observed, for the inverse setting, with *mt*Dod SpyC constructs, bands of unreacted scaffold monomer were visible (possibly caused by aggregation problems of the *mt*Dod SpyC constructs). We note that *mt*Dod SpyT/

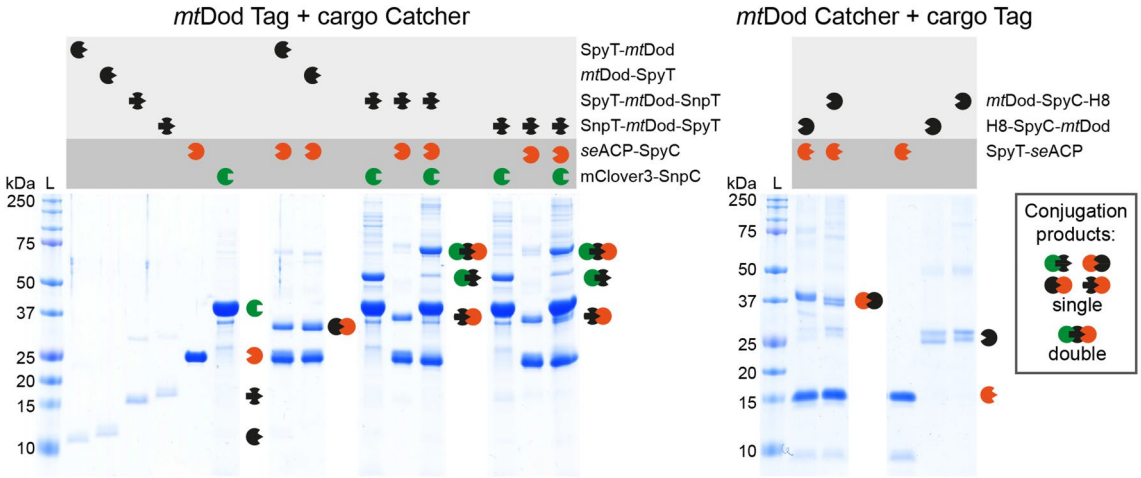

Figure 5. SDS-PAGE of the SpyT/-C and SnpT/-C reactions. Left: Reactions of *mt*Dod Spy-/SnpT constructs with *se*ACP-SpyC and/or mClover3-SnpC. Right: Inverse reactions of *mt*Dod SpyC constructs with SpyT-*se*ACP. In all reactions, bands of higher mass representing the conjugation products are observed. As mentioned above, the acidic loading buffer causes the appearance of double bands (*mt*Dod SpyC constructs) and smearing bands (*se*ACP-SpyC-H8) for some constructs.

SnpT constructs are lower in molecular mass than the *mt*Dod SpyC constructs, and traces of unreacted scaffold protein may be less visible on SDS-PAGE gels. This data shows that a high degree of saturation was achieved, indicating that SpyT/-C and SnpT/-C are well accessible at the *mt*Dod dodecamer scaffold. Double-tagged constructs SpyT-*mt*Dod-SnpT or SnpT-*mt*Dod-SpyT, heterovalently loaded with *se*ACP-SpyC and mClover3-SnpC, revealed bands of single-charged *mt*Dod monomers in SDS-PAGE. We explain this observation by an increased density at the surface of *mt*Dod that sterically constrains the conjugation with both cargos. Similar as the SpyT/-C and SnpT/-C constructs, also the SYNZIP constructs can be used for recruiting proteins to the *mt*Dod scaffold (although non-covalently). Due to the limited solubility and high aggregation tendencies of SYNZIP constructs, we only tested if *mt*Dod SYNZIP constructs are able to interact with the respective SYNZIP counterpart (e.g., *mt*Dod-SZ1 with SZ2-mClover3). For both *mt*Dod SYNZIP constructs, we observed the formation of *mt*Dod cargo adducts, indicated by higher apparent molecular mass peaks in SEC (Supplementary Fig. S8). This shows that also SYNZIP domains fused to *mt*Dod are functional and accessible. However, we deemed the SpyT/-C and SnpT/-C systems more suitable for *mt*Dod constructs, and did not further investigated the SYNZIP system.

In order to probe the accessibility and functionality of linked folds further, we tested the labelling of *mm*ACP linked to *mt*Dod with a 4′-phosphopantetheine CoA fluorophore mediated by the 4′-phosphopantetheine transferase from *Bacillus subtilis* (Sfp). The Sfp-mediated modification of ACP with CoA-modified fluorophores (CoA-488; ATTO-TEC dye ATTO 488) has been frequently used for the labelling of cellular compounds[36]. All reactions were conducted at 25 °C for 1 h in triplicates, and stopped by the addition of acidic loading buffer and analysed by SDS-PAGE. To determine the relative accessibility of *mm*ACP linked to *mt*Dod, fluorescence intensities of *mt*Dod-*mm*ACP and *mt*Dod-*mm*ACP-H8 were compared to free *mm*ACP after labelling (Fig. 6).

By comparing the fluorescence intensities of CoA-488-labeled *mt*Dod-*mm*ACP and *mt*Dod-*mm*ACP-H8 with CoA-488-labeled free *mm*ACP, the relative degree of labelling was determined to about 31% ± 8% and 36% ± 8% respectively. After an additional hour of labelling, in-gel fluorescence of *mt*Dod-*mm*ACP and of *mt*Dod-*mm*ACP-H8 further increased by 14% ± 8% and 24% ± 12%, respectively. The overall low relative degree of labelling and the increase after an additional hour of reaction time indicates a reduced accessibility of *mm*ACP fused to *mt*Dod. It cannot be ruled out that the *mm*ACP fold fused to *mt*Dod is instable or partly unfolded. Note that in SDS-PAGE, *mt*Dod-*mm*ACP runs at just two different apparent molecular weights corresponding to labelled and non-labelled protein (see Fig. 6). It seems that SDS-PAGE is limited in its efficiency of separating mixtures of unlabelled and labelled monomers.

***Mt*Dod-PAS-pep constructs for AB production.** Protein carriers are generally used for the production of ABs against peptides or proteins[9]. In the standard approach, the peptide or the protein of interest is linked to the carrier, usually BSA or KLH, by chemical ligation[8–10]. While the method is well-established and broadly used for AB production, problems can arise during conjugating the peptide/hapten to the carrier, e.g., owing to the low stability or solubility of the conjugate (or even for the peptide alone) or altered antigenic properties of the peptide[17]. The dodecameric structure with the exposed termini allows *mt*Dod to be charged with 12 or 24 peptides/proteins on its surface by simply fusing the peptide/protein encoding sequence to the *mt*Dod gene. In order to evaluate the suitability of *mt*Dod for AB production, 11 fusion constructs were produced in *E. coli* of which each is comprised of *mt*Dod, a PAS linker and a peptide of interest, termed *mt*Dod-PAS-Pep (Table 2). Peptide sequences originated from human heat shock proteins (HSP), proheparin-binding EGF-like growth factor (HB-EGF) and C-terminus of the heat shock cognate protein 70 interacting protein (CHIP) (for detailed peptide origin see Supplementary Table S2). Peptides/epitopes were selected, because of a specific scientific interest in

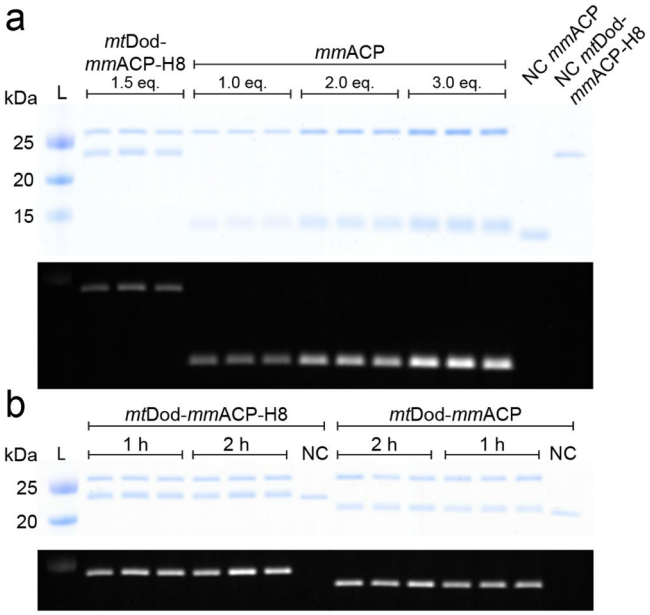

Figure 6. Modification of *mt*Dod-*mm*ACP, *mt*Dod-*mm*ACP-H8 and *mm*ACP by Sfp with fluorescent CoA. L: ladder. NC: negative control reaction without Sfp. Eq.: molar equivalents of *mm*ACP loaded onto the SDS-PAGE gel. (**a**) Top: Coomassie stained SDS-PAGE gel of the reaction solution and negative controls. Sfp, runs at an apparent molecular weight of slightly above 25 kDa, *mt*Dod-*mm*ACP-H8 slightly below 25 kDa and *mm*ACP slightly below 15 kDa. Unmodified *mm*ACP and *mt*Dod-*mm*ACP-H8 (negative controls) show lower apparent molecular weights indicating a different running behaviour between CoA-488 modified and unmodified proteins. Bottom: In-gel fluorescence taken before Coomassie staining. Only proteins modified with the CoA-488 are visible. Higher bands represent labelled *mt*Dod-*mm*ACP-H8 and lower bands labelled *mm*ACP. (**b**) Top: Coomassie stained SDS-PAGE gel of the reaction solutions of *mt*Dod-*mm*ACP-H8 and *mt*Dod-*mm*ACP after 1 h and 2 h. Bottom: in-gel fluorescence taken before Coomassie staining. For both constructs, fluorescence intensity increases at longer reaction times. For uncropped images and *mt*Dod-*mm*ACP blots see Supplementary Fig. S9.

*mt*Dod constructs	Peptide sequence	Calculated mass without start-Met/Da	Measured mass by MS (+1 H^+)/Da
*mt*Dod-PAS-Pep1	PKGGSGSGPTIEEVD	10,155	10,156.7
*mt*Dod-PAS-Pep2	PLEGDDDTSRMEEVD	10,434	10,435.0
*mt*Dod-PAS-Pep3	ECYPNEKNSVNMDLD	10,497	10,803.4*
*mt*Dod-PAS-Pep4	VPSDSDKKLPEMDID	10,415	10,416.1
*mt*Dod-PAS-Pep5	DSSQHTKSSGEMEVD	10,363	10,363.9
*mt*Dod-PAS-Pep6	EQSTGQKRPLKNDEL	10,469	10,470.2
*mt*Dod-PAS-Pep7**	ALMVYRCAPPRSSQF	10,453	–
*mt*Dod-PAS-Pep8	LVTGESLEQLRRGLA	10,368	10,369.1
*mt*Dod-PAS-Pep9	MKGKEEKEGGARLGA	10,287	10,288.0
*mt*Dod-PAS-Pep10	EERRIHQESE	10,038	10,039.6
*mt*Dod-PAS-Pep11	NHEGDEDDSH	9,880	9,881.3
*mt*Dod-PAS-H7	HHHHHHH	9,704	9,705.2

Table 2. *Mt*Dod constructs for AB production. After purification by the heat treatment protocol, the correct size of the proteins was verified by ESI–MS. *Difference of mass is about 305 Da and could be caused by S-glutathionylation[37,38], No mass for the unmodified *mt*Dod-PAS-Pep3 was observed. ***Mt*Dod-PAS-Pep7 formed inclusion bodies and was not purified.

the proteins carrying the peptides, and not for their sequence composition or the thermal stability properties of the source proteins (e.g. thermal stability of HSP). In that light, the case study presented here is also a "real case" for the applicability of the dodecin matrix.

Pep-encoding sequences, provided on oligonucleotide primers, were introduced in single-step by ligation-free cloning. Recombinant expressions and purifications followed the established protocols described above. All constructs were received as soluble proteins, except *mt*Dod-PAS-Pep7 that formed inclusion bodies (see Table 2).

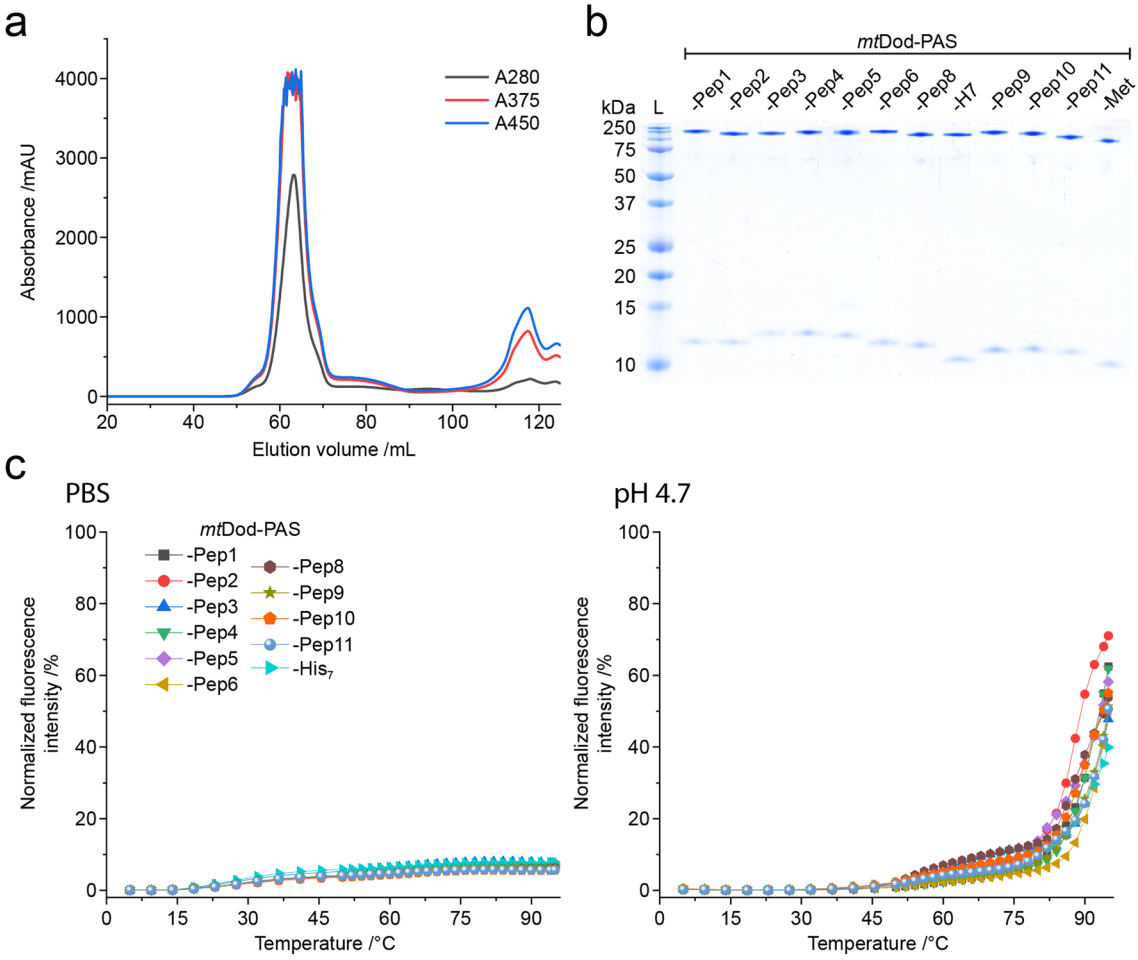

Figure 7. *Mt*Dod-PAS-Pep purity and stability. (**a**) SEC profile of FMN:*mt*Dod-PAS-Pep1. The dodecameric species can be identified by the FMN absorption at 375 nm and 450 nm. In addition, unbound FMN is visible at ~ 117 mL. All constructs, except *mt*Dod-PAS-Pep3, showed comparable chromatographic profiles. (**b**) SDS-PAGE gel of all purified *mt*Dod-PAS-Pep constructs. Use of standard loading buffer (pH 6.8, 2.5% SDS) at prolonged heat incubation (30 min, 95 °C) allows the observation of monomer and dodecamer. (**c**) Thermocyclic fluorescence assay of *mt*Dod-PAS-Pep constructs. Measurements were performed in PBS and at pH 4.7 as described above (see Fig. 4).

The yellow colour of the inclusion bodies indicated assembled dodecamer, and we assume that aggregation of *mt*Dod-PAS-Pep7 was induced by the cysteine in Pep7, forming disulfide-bridges between the dodecamers. All constructs, except *mt*Dod-PAS-Pep7, were further purified by two cycles of DMSO-induced precipitations. FMN was added before constructs were eventually forwarded to SEC to remove unbound FMN and remaining DMSO as well as to select for dodecameric species (Fig. 7a). We assumed that *mt*Dod remains saturated with FMN due to its high affinity and cooperative binding mode.[23] FMN-saturated *mt*Dod constructs (FMN:*mt*Dod constructs) can be determined in concentration by absorbance at 450 nm, and are amenable to stability measurements by the thermocyclic fluorescence assay. All constructs were received as dodecamers, as indicated by SEC (Supplementary Fig. S10). *Mt*Dod-PAS-Pep3 shows in addition to the dodecamer species higher oligomeric states in SEC, which we assume to result from disulfide-bridges formed by the cysteine in Pep3. The dodecamer containing fractions were pooled, and the purity was controlled by SDS-PAGE (see Fig. 7b). The thermocyclic fluorescence assay revealed the high thermal stability of all *mt*Dod-PAS-Pep constructs, similar as the wild type protein (Fig. 7c)[23]. Molecular masses of the constructs were measured with ESI–MS and confirmed full-length protein (see Table 2).

The amount of purified protein/dodecamer of *mt*Dod-PAS-Pep constructs were between 20–50 mg, purified from about 100 mL of the 500 mL expression culture (calculated yields of 200–500 mg per litre). The construct *mt*Dod-PAS-Pep3 was received at the lowest amount (about 20 mg; 200 mg/litre), which may be explained by agglomeration of dodecamers due to disulfide bridges. Constructs *mt*Dod-PAS-Pep3 and *mt*Dod-PAS-Pep7 indicate that cysteine containing peptides can cause problems when processed via the described purification strategy. A changed protocol, in which the oxidative conditions imposed by the high concentrations of FMN are avoided, could lead to improved results.

Endotoxin concentrations, measured in endotoxin units (EU) via a *Limulus* amebocyte lysate (LAL) test, were determined to avoid an endotoxin shock in immunizations. *Mt*Dod-PAS-Pep3 and Dod-PAS-Pep6 contained

ABs derived from *mt*Dod construct	Binding region of the ABs	AB class
*mt*Dod-PAS-Pep1	HSP-70 C-terminus	Class 1
*mt*Dod-PAS-Pep2	HSP-90 C-terminus	Class 1
*mt*Dod-PAS-Pep3	HSP-110 C-terminus	Class 1
*mt*Dod-PAS-Pep4	HSP-A4 C-terminus	Class 1
*mt*Dod-PAS-Pep5	H3 C-terminus	Class 2*
*mt*Dod-PAS-Pep6	H4 C-terminus	Class 3
*mt*Dod-PAS-Pep8	HB-EGF** Pos. 20–34	Class 3
*mt*Dod-PAS-Pep9	CHIP N-terminus	Class 1
*mt*Dod-PAS-Pep10	CHIP Broken helix Pos. 151–161	Class 2***
*mt*Dod-PAS-Pep11	CHIP Tip of helix Pos. 183–192	Class 1

Table 3. Classification of *mt*Dod-PAS-Pep derived ABs. ABs were classified as followed: "Class 1" ABs recognize the proteins of interest provided as recombinantly purified protein (produced in *E. coli*). "Class 2" ABs do not recognize recombinant protein of interest, but protein of expected apparent molecular weight in HEK293T human cell lysates. "Class 3" ABs only recognize *mt*Dod-PAS constructs (like the respective *mt*Dod-PAS-Pep or *mt*Dod-PAS-Met). Western blots of ABs rated as "class 1" or "class 2" are shown in Fig. 8. The AB derived from *mt*Dod-PAS-Pep6 and *mt*Dod-PAS-Pep8 only recognized *mt*Dod-PAS-Pep constructs and were considered "class 3" (Supplementary Fig. S11). **mt*Dod-PAS-Pep5 derived ABs showed only a very weak signal for 1 µg and 500 ng of recombinant protein with no intensity difference (see Supplementary Fig. S11). Thus, the AB preparation was regarded as "class 2". **Proheparin-binding EGF-like growth factor of *Chlorocebus aethiops* (green monkey). ****mt*Dod-PAS-Pep10 derived ABs didn't recognize purified CHIP but seem to recognize a protein in CHIP-overexpressing cells; no detection range was determined.

the highest amount of endotoxin with 73 EU/mg and 55 EU/mg, respectively; all other samples showed values less than 30 EU/mg (average of all constructs 30 ± 23 EU/mg). Since about 100 µg protein was used per injection, none of the samples were critical in endotoxin levels (above 5–10 EU/kg of rabbit per injection)[39,40].

Purified *mt*Dod constructs were eventually submitted to an AB production company for immunization in rabbits and AB purification (Davids Biotechnologie GmbH, Germany). AB productions were induced in one rabbit for each construct by 5 injections (about 100 µg each, *mt*Dod-PAS-Pep solution concentration: 2.2–7.5 mg/mL (average 4.5 ± 1.3 mg)) over 63 days using the adjuvant MF59/AddaVax. The ABs were purified from the collected serum by affinity chromatography with the respective *mt*Dod-PAS-Pep construct immobilized on the column matrix. For all the 10 *mt*Dod-PAS-Pep constructs, which were submitted to immunizations, purified ABs were obtained and their binding behaviour analysed by western blotting (summarized in Table 3).

The produced ABs did not create any reoccurring background signals indicating that the *mt*Dod-PAS carrier matrix does not cause the generation of ABs that recognize proteins present in lysate of HEK293T cells (see Fig. 8a, Supplementary Fig. S11 and Supplementary Fig. S12). This agrees with the low sequence identity of *mt*Dod-PAS with human proteins (protein–protein BLAST with default settings finds no human protein with significant similarity).

The six ABs rated as "class 1" were tested on different concentrations of target protein (1 µg to 60 ng) to estimate their general labelling capability in western blots (see Fig. 8b). Further, the same dilutions of target protein were used to give a rough comparison for *mt*Dod-PAS-Pep derived ABs with commercially available ABs (exception *mt*Dod-PAS-Pep2, for which we had no commercial AB to hand). In general, the *mt*Dod-PAS-Pep derived ABs were comparable with commercial ABs (see Fig. 8b), and are well suited for specific labelling of target protein in lysate samples.

The *mt*Dod-PAS-Pep-derived ABs show that *mt*Dod-PAS is a well-suited carrier system for the production of peptide-specific ABs. *Mt*Dod-PAS-based fusions benefit from the easy cloning, uncomplicated production/purification and the high protein yields. In our case study, problems in the purification of cysteine containing constructs emerged from the oxidative conditions induced by high FMN concentrations, which may, however, be overcome when working under reducing conditions. Alternatively, cysteine could be replaced by serine residues, as recommended by AB producing companies for epitopes containing internal cysteines, although this might alter the epitopes and affect the specificity of the produced ABs.

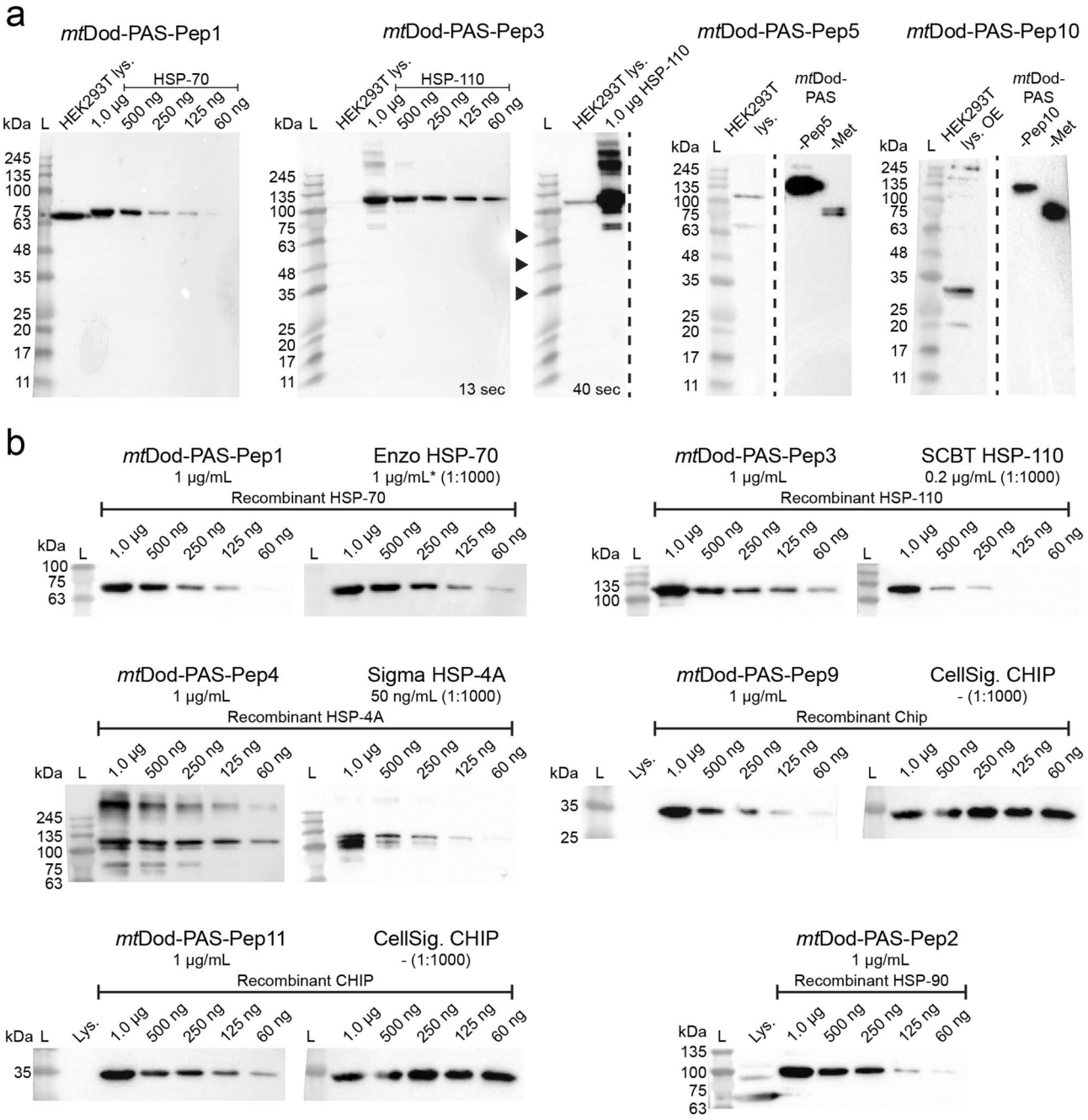

Figure 8. Western blots with selected *mt*Dod-PAS-Pep construct ABs. L: Ladder. Lys.: Lysate. OE: protein overexpressing cells. (**a**) Detection of the target protein in purified form and in the lysate. ABs derived from *mt*Dod-PAS-Pep1 and *mt*Dod-PAS-Pep3 detect target proteins in the lysate. For *mt*Dod-PAS-Pep3, the same blot is shown with two exposure times (13 s and 40 s) to make the potential HSP-110 representing band in the lysate observable. ABs derived from *mt*Dod-PAS-Pep5 and *mt*Dod-PAS-Pep10 did not recognize purified target protein, but seem to recognize a protein in overexpressing cells (uncropped western blots see Supplementary Fig. S11) (**b**) Comparison with commercially available ABs. Different amounts (1 µg to 60 ng) of purified target protein were loaded and analysed by *mt*Dod-PAS-Pep derived ABs (1 µg/mL) and commercially available ABs (recommended dilutions were used; concentration given when available). All used commercial ABs should recognize different epitopes than the *mt*Dod-PAS-Pep derived ABs, since the given epitope amino acid regions are not overlapping with the selected peptides. Enzo HSP-70: Monoclonal anti HSP70 AB (epitope region amino acids 436–503) from Enzo Life Science, GmbH. *: Concentration assumed based on older aliquots, since information is not given for the newer ones. SCBT HSP-110: Monoclonal anti HSP-105/HSP-110 AB (epitope region amino acids 187–512) from Santa Cruz Biotechnology, Inc. Sigma HSP-4A: Polyclonal anti HSP-4A AB (epitope region amino acids 639–748) from Sigma-Aldrich, Merck KGaA. CellSig. CHIP: Monoclonal anti CHIP AB (epitope region L36 surrounding amino acids (synthetic peptide, length not given)) from Cell Signaling Technology, Inc. For uncropped western blots, see Supplementary Fig. S12. ABs derived from *mt*Dod-PAS-Pep2 also recognize HSP-70. For a comparison of *mt*Dod-PAS-Pep1-3 derived ABs, see Supplementary Fig. S13.

Conclusion

During the last years, dodecins have been characterized as flavin binding proteins involved in flavin homeostasis[21,23]. In addition, the unique protein fold and particularly the exceptional flavin binding mode were harnessed in technological applications, although exclusively on the archaeal protein from *Halobacterium salinarum*[41,42]. In this study, we present *mt*Dod as a versatile scaffold protein to attach peptides and small proteins.

The *mt*Dod dodecamer tolerates high temperatures and various chemical conditions, which allows protein purification by quick heat-induced denaturation and protein precipitation with solvents, and holds out the prospect that *mt*Dod broadly accept conditions for chemical ligation reactions. In addition to its high stability, *mt*Dod can be produced in high amounts in *E. coli*. For soluble constructs, yields of up to several hundred milligrams of *mt*Dod-peptide fusions per litre of bacterial culture can be expected. Proteins fused to *mt*Dod are presented at the *mt*Dod outer surface, and have been shown to remain accessible and functional. Both the SpyT/-C and the ACP/Sfp system allowed attaching the cargo at the *mt*Dod surface. In this respect, *mt*Dod is comparable to the recently presented IMX313 scaffold, suggested for use in vaccine development[19]. When evaluating *mt*Dod as a scaffold, we observed that constructs can suffer from low solubility in response to the properties of the attached cargo. While agglomeration by disulfide formation, observed for *mt*Dod-PAS-Pep3 and *mt*Dod-PAS-Pep7, could simply be avoided by reducing conditions during protein preparation or replacing of cysteine with serine residues, solubility problems induced by hydrophobic and structurally unstable fold may be solved by heterododecamer formation to dilute the aggregation-inducing species on the *mt*Dod surface. For the construct *mt*Dod-PAS-Strep, we demonstrated that heterododecamer formation with the wild type protein is readily possible in vitro and in vivo by simply providing both proteins during refolding or recombinant protein production, respectively (see Fig. 3).

As a pilot run for evaluating the suitability of *mt*Dod as a carrier matrix for AB production, we chose 11 peptides originating from different human proteins like CHIP or HSP-70, and fused them to *mt*Dod. One of the 11 peptide constructs formed inclusion bodies, while all other constructs were purified by the standard heat-denaturation purification protocol without any need for individual optimization. From all immunizations performed in this study, ABs were received that at least recognized the *mt*Dod-PAS scaffold in western blotting. Overall, 8 of the 10 ABs recognized proteins in HEK293T human cell lysate at expected molecular weight. For 6 of them, correct target recognition could be confirmed with the recombinantly purified protein as reference. No AB preparation showed any unspecific reactivity in HEK293T cell lysate, demonstrating that *mt*Dod is a suitable matrix for the production of ABs that specifically label the proteins of interest (in the HEK293T lysate) without the need to remove anti-carrier ABs. The low sequence identity of *mt*Dod to human proteins and eukaryotic proteins in general suggests that ABs derived from *mt*Dod will also be specific to proteins of interest in other human samples/cells[20,24].

The here presented AB production strategy with *mt*Dod may be attractive for labs that are experienced in protein expression, and want to produce ABs targeting peptides without relying on peptide synthesis and chemical crosslinking. We expect that the exposed termini are also suited for chemical ligation of haptens or antigens, following standard immunization protocols, or for Click chemical modification[43]. However, in proofing the concept of dodecin for peptide immunizations, we did not elaborate on this further. Finally, we note that the availability of dodecins with similar features (e.g. *Streptomyces coelicolor*, *Streptomyces davaonensis* and *Thermus thermophilus* dodecins)[22,44] is advantageous when aiming for heterologous prime/boost protocols by using two dodecin scaffolds with low sequence identity fused with the same antigen[45].

While the *mt*Dod has been mainly tested as carrier matrix for AB production in this study, the properties of *mt*Dod call for its application as a scaffold in a broad range of biotechnological and bioengineering applications. We encourage to explore the *mt*Dod as a scaffold when defined particles with specific surface properties are required. Such constructs can be valuable in e.g. diffusion measurements,[46] for formation of biomaterials[47–50] and in creating enzyme scaffolds[35,51,52]. *Mt*Dod heterododecamers may be applied for pull down assays when combining a *mt*Dod construct bearing a protein recruiting peptide and a *mt*Dod construct with a purification tag.

Material and methods

Cloning. Expression constructs were cloned using standard PCR methods and In-Fusion HD Cloning (TaKaRa Bio Europe). Primers were ordered from Sigma-Aldrich. Inserts were verified by Sanger sequencing (by Microsynth Seqlab, Göttingen, Germany). For polycistronic constructs spacer DNA sequences (between genes) were designed with EGNAS (version 1,158)[53]. For a list of all constructs see Supplementary Table S1.

Expression and cell lysis. Plasmids were transformed into BL21 (DE3) Gold cells and cells were plated onto LB-agar plates containing 100 ng/µL ampicillin and 1 g/mL glucose. 10 mL LB medium with 100 ng/µL ampicillin and 1 g/mL glucose were inoculated with a single colony and incubated at 37 °C and 180 rpm overnight. 1 L TB medium with 100 ng/µL ampicillin was inoculated with 10 mL overnight LB culture, and incubated at 37 °C and 180 rpm until the OD_{600} reached about 0.8. The cultures were cooled to 20–30 °C, and the expression was induced with 1 mL 1 M IPTG solution. The cultures were incubated overnight at 20 °C 160 rpm for protein production. *Mt*Dod-PAS-Pep constructs were expressed in 500 mL TB medium induced with 500 µL 1 M IPTG. Cells were harvested at 4,000 rcf and frozen in liquid nitrogen or directly processed. For purification by heat denaturation (*mt*Dod constructs), cell pellets were resuspended in 30 mL standard dodecin buffer: 300 mM NaCl, 5 mM $MgCl_2$ and 20 mM Tris–HCl (pH 7.4, adjusted with HCl). For purification by His-tag affinity chromatography, cell pellets were resuspended in 30 mL Ni–NTA wash buffer I: 200 mM NaCl, 35 mM K_2HPO_4 and 15 mM KH_2PO_4 (pH 7.4, adjusted with NaOH or HCl) and 40 mM imidazole. To the resuspended cells, PMSF and DNase I were added, and cells were disrupted by French press. Cell debris was removed by centrifugation (50,000 rcf, 20 min). All steps after cell harvest were conducted at 4 °C or on ice.

Purification by heat denaturation. The cell debris free lysates (about 30 mL) were divided in about 10 mL aliquots and incubated at 75 °C for 15 min. Lysate containing *mt*Dod-*mm*ACP or *mt*Dod-msfGFP-H8 was incubated at 55 °C or 70 °C, respectively. Heat-denatured proteins were removed by centrifugation (15,000 rcf, 10 min). Proteins in the supernatant (combined from 3 aliquots 20–25 mL) were precipitated with 50% (v/v) DMSO (final concentration) and pelleted by centrifugation (15,000 rcf, 10 min). Depending on the construct, higher concentrations or other organic solvents (MeOH and acetone) might be needed (precipitation with 75% (v/v) acetone (final concentration) turned out to be fastest and most reliable but might cause aggregation). The obtained protein pellets were dissolved in about 20 mL standard dodecin buffer at RT and afterwards cooled on ice. Precipitation was repeated once, and the pellets were dissolved in about 5 mL. Insoluble precipitate was removed by centrifugation (15,000 rcf, 10 min). To the protein solutions, FMN was added in excess (above its solubility limit) (F6750, Sigma-Aldrich: 70% pure, free RbF ≤ 6%) and samples were incubated on ice for at least 1 h. About 250–500 µL of protein solution were further purified by SEC. For loading the column, the concentration of the protein solution was judged by the yellow tone of the solution (depending on the dodecin concentration FMN solution turn from yellow to orange-brown).

Purification by His-tag affinity chromatography. The cleared lysate was poured on 5 mL packed Ni–NTA agarose (His60 Superflow, TaKaRa Bio Europe) gravity flow columns, pre-equilibrated with Ni–NTA wash buffer. The loaded resin was washed with 15 mL Ni–NTA wash buffer I and with 15 mL Ni–NTA wash buffer II (Ni–NTA wash buffer I with 80 mM imidazole). *Mt*Dod-msfGFP-H8 was additionally washed with 10 mL Ni–NTA wash buffer III (Ni–NTA wash buffer I with 200 mM imidazole). Proteins were eluted in 15 mL elution buffer (200 mM NaCl, 35 mM K_2HPO_4 and 15 mM KH_2PO_4 (pH 7.4, adjusted with NaOH or HCl) and 500 mM imidazole). Eluted proteins were concentrated with ultra centrifugal filters (Amicon, Merck) with the appropriated mass cut-off and further purified by SEC.

Refolding of *mt*Dod-*se*ACP, *mt*Dod SpyC and *mt*Dod SYNZIP constructs. Yellowish inclusion bodies obtained after cell disruption and centrifugation (50,000 rcf, 30 min) were manually separated from other solid cell debris and then washed three times (resuspended and centrifuged) with inclusion body wash buffer (137 mM NaCl, 2.7 mM KCl, 10 mM Na_2HPO_4, 0.5 mM KH_2PO_4 (PBS, pH 7.4 not adjusted), 5 mM EDTA and 2% (v/v) Triton X-100). The washed inclusion bodies were then dissolved in 10 mL GdmCL buffer (6 M guanidinium hydrochloride, 20 mM Tris–HCl (pH 8.0, adjusted with HCl)). For refolding, 0.5 mL protein solution were diluted with 4.5 mL GdmCL buffer containing L-Arginine (1 M final concentration). Refolding was performed by dialyzing twice against the 100-fold volume of the respective buffer containing 1 mM FMN (omitted for *mt*Dod SYNZIP constructs). For SpyC constructs, a phosphate borate buffer (100 mM NaCl 25 mM Na_2HPO_4, 25 mM H_3BO_3 (pH 8.5 adjusted with NaOH) and 20% glycerol) was used, and for all other constructs the standard dodecin buffer was used. Dialysis was conducted at 4 °C and without stirring for the first ~ 12 h (overnight). Aggregated protein was removed from the solution by centrifugation (3,000 rcf, 10 min). Refolded proteins were concentrated with ultra centrifugal filters (Amicon, Merck) with the appropriate mass cut-off and further purified by SEC.

SEC. Prior to injection, all samples were filtered with 0.22 µm membrane filters (Durapore, Merck). All proteins in this study, except *mt*Dod-PAS-Pep constructs, were purified by using an equilibrated Superdex 200 increase 10/300 column (GE Healthcare) on an ÄKTA Explorer or ÄKTA Basic device. For *mt*Dod-PAS-Pep constructs, a HiLoad Superdex 200 16/600 pg was used. Running buffer for all constructs, except *mt*Dod SpyC constructs and *mt*Dod-msfGFP-H8, was the standard dodecin buffer. The flow rate was 0.5 mL/min for the Superdex 200 increase 10/300 column or 1.0 mL/min for the HiLoad Superdex 200 16/600 pg column with fraction resolution of 0.3 mL or 2.0 mL, respectively. The running buffer for the *mt*Dod SpyC constructs and *mt*Dod-msfGFP-H8 was phosphate borate buffer (as used for refolding), and the flow rate was reduced to 0.45 mL. All runs were conducted at 4 °C. Fractions were pooled and analysed by SDS-PAGE with Coomassie staining. Pooled fractions were aliquoted, frozen in liquid nitrogen and stored at − 80 °C.

Protein concentrations. The concentration of FMN saturated *mt*Dod constructs was determined by the FMN absorption and the corresponding extinction coefficients (375 nm, 450 nm, 473 nm respective extinction coefficients 10,000 $M^{-1} \times cm^{-1}$, 12,000 $M^{-1} \times cm^{-1}$ and 9,200 $M^{-1} \times cm^{-1}$). The concentration of fluorescent proteins were determined by the chromophore absorption and the corresponding extinction coefficient (mClover3 constructs: 506 nm, 109,000 $M^{-1} \times cm^{-1}$ (ref[54]), mRuby3 constructs: 558 nm, 128,000 $M^{-1} \times cm^{-1}$ (ref[54]), msfGFP constructs: 485 nm 82,400 $M^{-1} \times cm^{-1}$ (ref[29])). For other proteins, the concentrations were determined by the absorption at 280 nm and applying the calculated extinction coefficient. For proteins with low amounts of bound flavin, the absorption at 280 nm was corrected using the absorptions at 450 nm and the 280/450 nm ratio of pure FMN.

SDS-PAGE. SDS-PAGE was performed at initial 70 V (15 min) followed by 200 V (about 70 min) on Tris-tricine gels (self-casted 10% gels, as described in ref[55] using an Mini-PROTEAN Tetra Cell system (Bio-Rad Laboratories, Inc.). For heterododecamer samples Tris-tricine (Laemmli) gels (self-casted 12% gels) and SDS free loading buffer (4×: 50% glycerol, 5 mM FMN) were used. Laemmli SDS-PAGE was performed at initial 70 V (15 min) followed by 200 V (about 150 min). For non-*mt*Dod construct samples or if full dodecamer denaturation was not necessary/wanted, standard SDS-PAGE loading buffer (4×: 50% (v/v) glycerol, 375 mM Tris–HCl (pH 6.8, adjusted with HCl), 10% (w/v) SDS, 10% (v/v) 2-mercaptoethanol, 50 mM EDTA, bromophenol

blue) was used. For full denaturation of the *mt*Dod dodecamer, a 2-component acidic SDS-PAGE loading buffer (4 × acidic part 1: 10% (w/v) SDS, 300 mM acetic acid; 4 × acidic part 2: 50% (v/v) glycerol, 300 mM Tris (unbuffered), 200 mM Tris–HCl (pH 6.8, adjusted with HCl), 10% (v/v) 2-mercaptoethanol, 50 mM EDTA, bromophenol blue) was used. Amount of acetic acid and unadjusted Tris can be varied together if needed. Samples were mixed with the standard SDS-PAGE loading buffer or acidic SDS-PAGE loading buffer component 1 and heat treated at 95 °C (10 min). After heat treatment, acidic SDS-PAGE loading buffer component 2 was added to the acidic samples and a second heat treatment was applied. Gels were stained over night with InstantBlue Coomassie stain (Expedeon) and imaged using a scanner (Epson Expression 1,680 Pro, Seiko Epson Corporation).

Thermocyclic fluorescence assay. For stability measurements, a clear 96 well PCR plate (MLL9601; Bio-Rad Laboratories, Inc.) was prefilled with 23 µL of respective buffer per well; i.e., PBS or acetate buffer (150 mM NaCl, 100 mM acetic acid (pH 4.2, adjusted with NaOH)). Plates were placed on ice and 2 µL of the corresponding 50 mM *mt*Dod construct solution were added to the wells. Plates were then sealed with optical tape (iCycler iQ; Bio-Rad Laboratories, Inc.), centrifuged (3,000 rcf, 2 min) and placed into a precooled (5 °C) real-time PCR instrument (C1000 Thermal Cycler and CFX96 Real-Time System; Bio-Rad Laboratories, Inc.). For the fluorescence detection, excitation/emission filter bandwidth of 450–490/560–580 nm was used. After 1 h incubation at 5 °C, the heating and cooling cycles were started, with each cycle containing a heating phase for 6 min and a cooling (5 °C) phase for 30 min. The heating phase temperature was raised stepwise from 5 °C to 95 °C. Until 50 °C, the step size was 4.5 °C while at higher temperatures the step size was reduced to 2.0 °C. Data points were taken after each phase. The complete temperature protocol was applied to every sample. For the stability measurements of *mt*Dod-PAS-Pep constructs, the acetate buffer was replaced with a MES buffer (150 mM NaCl, 100 mM MES (pH 4.7, adjusted with HCl) and the heating phase duration was prolonged to 10 min.

Modification of *mm*ACP, *mt*Dod-*mm*ACP and *mt*Dod-*mm*ACP-H8 with Sfp. Sfp used for phosphopantetheinylation was produced in *E. coli* (Strain M15; helper plasmid pREP4 and pQE-60 encoding Sfp) and purified by His-tag affinity chromatography, dialysis overnight against imidazole free buffer (250 mM NaCl, 2 mM $MgCl_2$, 10% glycerol, 50 mM HEPES (pH 8.0 adjusted with HCl)) and SEC (HiLoad Superdex 200 16/60 pg)[56]. Holo *mm*ACP was produced in *E. coli* and purified by His-tag affinity chromatography (basic buffer: 200 mM NaCl, 35 mM K_2HPO_4 and 15 mM KH_2PO_4 (pH 7.4, adjusted with NaOH or HCl), 10% glycerol; washing buffer contained 20 mM imidazole and elution buffer contained 300 mM imidazole) and SEC (HiLoad Superdex 75 16/60 pg), similar as described for ACP-GFP by Heil and Rittner et al.[57] Pooled SEC fractions of Sfp and *mm*ACP were aliquoted, frozen in liquid nitrogen and stored at − 80 °C. The modification of *mm*ACP and *mt*Dod-*mm*ACP (both variants with H8-Tag and without) with CoA 488 (CoA modified with ATTO-TEC dye ATTO 488, NEB #S9348) by Sfp was conducted in phosphate borate buffer (pH 7.4, adjusted with HCl) at 25 °C for 1 h at following conditions: 10 µM *mt*Dod-*mm*ACP or *mm*ACP, 4 µM Sfp, 1 mM DTT, 10 mM $MgCl_2$ and 10 µM CoA 488. The final reaction volume was 50 µL, and reactions were carried out in triplicates. For calibration of the fluorescent signals, 3 different amounts of each *mm*ACP-H8 reaction solution (1 µL, 2 µL, 3 µL) were analysed.1.5 µL of the corresponding *mt*Dod-*mm*ACP construct reaction solution were used for the determination of the degree of labelling. The reaction mixtures were by analysed by SDS-PAGE, in-gel fluorescence, using the Fusion SL2 Xpress imaging system (Vilber Lourmat GmbH) with the emission filter F-595 Y3 (520–680 nm), and Coomassie staining. For quantification of fluorescence signals, the Fusion-Capt Advance SL2 Xpress 16.08a software (Vilber Lourmat GmbH) was used. The degree of modification of *mt*Dod-*mm*ACP was determined by linear regression of the normalized (by molar amount) fluorescence signals.

SpyC and SnpC reactions. The reactions were carried out in phosphate borate buffer (pH 8.5) at 25 °C for 20 h. Concentration of the respective carrier constructs were 10 µM (1 eq.) and 20 µM of the respective cargo constructs (2 eq.), reaction volume was 50 µL. Each protein also was separately prepared in the same concentration as used in the reaction and incubated under the same conditions. 5 µL of each reaction and control were analysed by SDS-PAGE and Coomassie staining, for all samples the acidic loading buffer was used.

LC–MS. For the LC–MS analysis of the *mt*Dod-PAS-Pep constructs, 500 µg protein were precipitated with 75% (v/v) acetone (− 20 °C, final concentration), pelleted by centrifugation (20,000 rcf, 5 min) and dissolved in 100 µL water. After removal of undissolved aggregates by centrifugation (20,000 rcf, 5 min), the solution was diluted with 5% (v/v) acetonitrile:water to a final concentration of 0.1 mg/mL. The injection/sample size was 2.5 µL (250 ng). Samples were analysed by using a Dionex UltiMate 3,000 RSLC (Thermo Fischer Scientific) coupled to a micrOTOF-Q II (Bruker Daltonik GmbH) equipped with an electrospray ionization source. Chromatographic separation (further desalting) was performed on a Discovery BIO Wide Pore C5 column (100 × 2.1 mm, particle size 3 µm, Sigma-Aldrich) at 55 °C with a mobile-phase system consisting of water and acetonitrile (each containing 0.1% formic acid). A linear gradient ranging from 5 to 95% acetonitrile over 14 min at a flow rate of 0.4 mL min^{-1} was used. MS data was acquired in positive mode in the range from 200–2,500 m/z and later analysed using Compass DataAnalysis 4.0 software (Bruker Daltonik GmbH).

Western blots. Samples separated by SDS-PAGE were transferred to 0.45 µm nitrocellulose membranes at 100 V for 35–40 min in a cooled Criterion Blotter filled with transfer buffer at 4 °C (transfer buffer: 25 mM Tris, 192 mM glycine, 20% (v/v) methanol). Membranes were blocked in 5% (w/v) milk powder in TBS (50 mM Tris–HCl pH 7.6, 150 mM NaCl) with 0.1% Tween-20 added (TBST) for 1 h at RT, before addition of primary AB in indicated dilutions and incubation over night at 4 °C. Used primary ABs: Enzo HSP-70: #ADI-SPA-810 Enzo Life Science GmbH; SCBT HSP-110: #sc-74550 Santa Cruz Biotechnology, Inc.; Sigma HSP-4A: #HPA010023

Sigma-Aldrich, Merck KGaA; CellSig. CHIP: #2080 Cell Signaling Technology, Inc. Membranes were washed twice with TBST, followed by addition of secondary AB (#A4416 or #A9169 Sigma-Aldrich, Merck KGaA) in a 1:3,000 dilution in blocking buffer for 1 h at RT. Finally, membranes were washed twice with TBST. Chemiluminescence was developed with SuperSignal West Pico PLUS, and images were acquired with a ChemiDoc MP imaging system and quantified using Image Lab 5.0 software (Bio-Rad Laboratories, Inc.). Recombinant proteins used for AB comparison were produced in *E. coli* and purified by affinity chromatography and SEC. Proteins HSP-70, HSP-90, HSP-110 and HSP-A4 were expressed based on pPROEX vector system with a N-terminal His-tag that was removed by a TEV protease after affinity chromatography. CHIP was expressed based on a pGEX-6P1 vector system with a N-terminal GST-tag that was removed by the PreScission protease after affinity chromatography. All ABs were stored at − 20 °C prior use.

Received: 19 March 2020; Accepted: 13 July 2020
Published online: 06 August 2020

References

1. Tolar, P., Hanna, J., Krueger, P. D. & Pierce, S. K. The constant region of the membrane immunoglobulin mediates B cell-receptor clustering and signaling in response to membrane antigens. *Immunity* **30**, 44–55 (2009).
2. Bachmann, M. F. & Zinkernagel, R. M. Neutralizing antiviral B cell responses. *Annu. Rev. Immunol.* **15**, 235–270 (1997).
3. Chauhan, V., Rungta, T., Goyal, K. & Singh, M. P. Designing a multi-epitope based vaccine to combat Kaposi Sarcoma utilizing immunoinformatics approach. *Sci. Rep.* **9** (2019).
4. Schubert, B. & Kohlbacher, O. Designing string-of-beads vaccines with optimal spacers. *Genome Med.* **8** (2016).
5. Bennett, N. R., Zwick, D. B., Courtney, A. H. & Kiessling, L. L. Multivalent antigens for promoting B and T cell activation. *ACS Chem. Biol.* **10**, 1817–1824 (2015).
6. Mariani, M. *et al.* Immunogenicity of a free synthetic peptide: Carrier-conjugation enhances antibody affinity for the native protein. *Mol. Immunol.* **24**, 297–303 (1987).
7. Sanchez-Trincado, J. L., Gomez-Perosanz, M. & Reche, P. A. Fundamentals and methods for T- and B-cell epitope prediction. *J. Immunol. Res.* **2017**, 2680160 (2017).
8. Grant, G. A. Synthetic peptides for production of antibodies that recognize intact proteins. *Curr. Protoc. Mol. Biol.* **59**, 11.16.1-11.16.19 (2002).
9. Trier, N. H., Hansen, P. R. & Houen, G. Production and characterization of peptide antibodies. *Methods* **56**, 136–144 (2012).
10. Peeters, J. M., Hazendonk, T. G., Beuvery, E. C. & Tesser, G. I. Comparison of four bifunctional reagents for coupling peptides to proteins and the effect of the three moieties on the immunogenicity of the conjugates. *J. Immunol. Methods* **120**, 133–143 (1989).
11. Sakarellos-Daitsiotis, M., Krikorian, D., Panou-Pomonis, E. & Sakarellos, C. Artificial carriers: a strategy for constructing antigenic/immunogenic conjugates. *Curr. Top. Med. Chem.* **6**, 1715–1735 (2006).
12. Hume, H. K. C. *et al.* Synthetic biology for bioengineering virus-like particle vaccines. *Biotechnol. Bioeng.* **116**, 919–935 (2019).
13. Singh, K. V., Kaur, J., Varshney, G. C., Raje, M. & Suri, C. R. Synthesis and characterization of hapten–protein conjugates for antibody production against small molecules. *Bioconjug. Chem.* **15**, 168–173 (2004).
14. Adamczyk, M. *et al.* Characterization of protein-hapten conjugates. 1. matrix-assisted laser desorption ionization mass spectrometry of immuno BSA-hapten conjugates and comparison with other characterization methods. *Bioconjug. Chem.* **5**, 631–635 (1994).
15. Harris, J. R. & Markl, J. Keyhole limpet hemocyanin (KLH): a biomedical review. *Micron* **30**, 597–623 (1999).
16. Swaminathan, A., Lucas, R. M., Dear, K. & McMichael, A. J. Keyhole limpet haemocyanin—a model antigen for human immunotoxicological studies. *Br. J. Clin. Pharmacol.* **78**, 1135–1142 (2014).
17. Briand, J. P., Muller, S. & Van Regenmortel, M. H. V. Synthetic peptides as antigens: Pitfalls of conjugation methods. *J. Immunol. Methods* **78**, 59–69 (1985).
18. Brune, K. D. *et al.* Plug-and-display: decoration of virus-like particles via isopeptide bonds for modular immunization. *Sci. Rep.* **6**, 19234 (2016).
19. Brune, K. D. *et al.* Dual plug-and-display synthetic assembly using orthogonal reactive proteins for twin antigen immunization. *Bioconjug. Chem.* **28**, 1544–1551 (2017).
20. Bieger, B., Essen, L.-O. & Oesterhelt, D. Crystal structure of halophilic Dodecin: a novel, dodecameric flavin binding protein from *Halobacterium salinarum*. *Structure* **11**, 375–385 (2003).
21. Grininger, M., Staudt, H., Johansson, P., Wachtveitl, J. & Oesterhelt, D. Dodecin is the key player in flavin homeostasis of Archaea. *J. Biol. Chem.* **284**, 13068–13076 (2009).
22. Meissner, B., Schleicher, E., Weber, S. & Essen, L. O. The dodecin from *Thermus thermophilus*, a bifunctional cofactor storage protein. *J. Biol. Chem.* **282**, 33142–33154 (2007).
23. Bourdeaux, F. *et al.* Flavin storage and sequestration by *Mycobacterium tuberculosis* dodecin. *ACS Infect. Dis.* **4**, 1082–1092 (2018).
24. Liu, F. *et al.* Structural and biophysical characterization of *Mycobacterium tuberculosis* Dodecin Rv1498A. *J. Struct. Biol.* **175**, 31–38 (2011).
25. Zakeri, B. *et al.* Peptide tag forming a rapid covalent bond to a protein, through engineering a bacterial adhesin. *Proc. Natl. Acad. Sci.* **109**, E690–E697 (2012).
26. Li, L., Fierer, J. O., Rapoport, T. A. & Howarth, M. Structural analysis and optimization of the covalent association between spycatcher and a peptide tag. *J. Mol. Biol.* **426**, 309–317 (2014).
27. Veggiani, G. *et al.* Programmable polyproteams built using twin peptide superglues. *Proc. Natl. Acad. Sci.* **113**, 1202–1207 (2016).
28. Thompson, K. E., Bashor, C. J., Lim, W. A. & Keating, A. E. SYNZIP protein interaction toolbox: in vitro and in vivo specifications of heterospecific coiled-coil interaction domains. *ACS Synth Biol* **1**, 118–129 (2012).
29. Pédelacq, J.-D., Cabantous, S., Tran, T., Terwilliger, T. C. & Waldo, G. S. Engineering and characterization of a superfolder green fluorescent protein. *Nat. Biotechnol.* **24**, 79 (2006).
30. Schlapschy, M. *et al.* PASylation: a biological alternative to PEGylation for extending the plasma half-life of pharmaceutically active proteins. *Protein Eng. Des. Sel.* **26**, 489–501 (2013).
31. Jevševar, S. *et al.* Production of nonclassical inclusion bodies from which correctly folded protein can be extracted. *Biotechnol. Prog.* **21**, 632–639 (2005).
32. Ishii, M., Kunimura, J. S., Jeng, H. T., Penna, T. C. V. & Cholewa, O. Evaluation of the pH-and thermal stability of the recombinant green fluorescent protein (GFP) in the presence of sodium chloride. In *Applied Biochemistry and Biotecnology*, 555–571 (Springer, Berlin, 2007).
33. Shieh, Y.-W. *et al.* Operon structure and cotranslational subunit association direct protein assembly in bacteria. *Science* **350**, 678–680 (2015).
34. Grininger, M., Zeth, K. & Oesterhelt, D. Dodecins: a family of lumichrome binding proteins. *J. Mol. Biol.* **357**, 842–857 (2006).

35. Lili, J., Kosuke, M., Hirofumi, I., Kouhei, T. & Noriho, K. Polymeric SpyCatcher scaffold enables bioconjugation in a ratio-controllable manner. *Biotechnol. J.* **12**, 1700195 (2017).
36. Yin, J., Lin, A. J., Golan, D. E. & Walsh, C. T. Site-specific protein labeling by Sfp phosphopantetheinyl transferase. *Nat. Protoc.* **1**, 280–285 (2006).
37. Hill, B. G., Ramana, K. V., Cai, J., Bhatnagar, A. & Srivastava, S. K. Measurement and identification of s-glutathiolated proteins. *Methods Enzymol.* **473**, 179–197 (2010).
38. Zhang, H. *et al.* Glutathionylation of the bacterial Hsp70 chaperone dnak provides a link between oxidative stress and the heat shock response. *J. Biol. Chem.* **291**, 6967–6981 (2016).
39. Wachtel, R. E. & Tsuji, K. Comparison of limulus amebocyte lysates and correlation with the United States pharmacopeial pyrogen test. *Appl. Environ. Microbiol.* **33**, 1265–1269 (1977).
40. Pearson, F. C. *et al.* Comparison of several control standard endotoxins to the National Reference Standard Endotoxin–an HIMA collaborative study. *Appl. Environ. Microbiol.* **50**, 91–93 (1985).
41. Nöll, G., Trawöger, S., von Sanden-Flohe, M., Dick, B. & Grininger, M. Blue-light-triggered photorelease of active chemicals captured by the flavoprotein Dodecin. *ChemBioChem* **10**, 834–837 (2009).
42. Gutiérrez Sánchez, C., Su, Q., Schönherr, H., Grininger, M. & Nöll, G. Multi-ligand-binding flavoprotein Dodecin as a key element for reversible surface modification in nano-biotechnology. *ACS Nano* **9**, 3491–3500 (2015).
43. Kolb, H. C., Finn, M. G. & Sharpless, K. B. Click chemistry: diverse chemical function from a few good reactions. *Angew. Chem. Int. Ed.* **40**, 2004–2021 (2001).
44. Bourdeaux, F. *et al.* Comparative biochemical and structural analysis of the flavin-binding Dodecins from *Streptomyces davaonensis* and Streptomyces coelicolor reveals striking differences with regard to multimerization. *Microbiology* https://doi.org/10.1099/mic.0.000835 (2019).
45. Lu, S. Heterologous prime-boost vaccination. *Curr. Opin. Immunol.* **21**, 346–351 (2009).
46. Gutiérrez Sánchez, C., Su, Q., Wenderhold-Reeb, S. & Nöll, G. Nanomechanical properties of protein–DNA layers with different oligonucleotide tethers. *RSC Adv.* **6**, 56467–56474 (2016).
47. Chen, A. Y. *et al.* Synthesis and patterning of tunable multiscale materials with engineered cells. In *Nature materials* (2014). https://doi.org/10.1038/nmat3912.
48. Botyanszki, Z., Tay, P. K. R., Nguyen, P. Q., Nussbaumer, M. G. & Joshi, N. S. Engineered catalytic biofilms: site-specific enzyme immobilization onto *E. coli* curli nanofibers. *Biotechnol. Bioeng.* **112**, 2016–2024 (2015).
49. Sun, F., Zhang, W.-B., Mahdavi, A., Arnold, F. H. & Tirrell, D. A. Synthesis of bioactive protein hydrogels by genetically encoded SpyTag-SpyCatcher chemistry. *Proc. Natl. Acad. Sci.* **111**, 11269–11274 (2014).
50. Fletcher, J. M. *et al.* Self-assembling cages from coiled-coil peptide modules. *Science* **340**, 595–599 (2013).
51. Giessen, T. W. & Silver, P. A. A catalytic nanoreactor based on in vivo encapsulation of multiple enzymes in an engineered protein nanocompartment. *ChemBioChem* **17**, 1931–1935 (2016).
52. Siu, K.-H. *et al.* Synthetic scaffolds for pathway enhancement. *Curr. Opin. Biotechnol.* **36**, 98–106 (2015).
53. Kick, A., Bönsch, M. & Mertig, M. EGNAS: an exhaustive DNA sequence design algorithm. *BMC Bioinform.* **13**, 138 (2012).
54. Bajar, B. T. *et al.* Improving brightness and photostability of green and red fluorescent proteins for live cell imaging and FRET reporting. *Sci. Rep.* **6**, 20889 (2016).
55. Schägger, H. Tricine–SDS-PAGE. *Nat. Protoc.* **1**, 16–22 (2006).
56. Mofid, M. R., Marahiel, M. A., Ficner, R. & Reuter, K. Crystallization and preliminary crystallographic studies of Sfp: a phosphopantetheinyl transferase of modular peptide synthetases. *Acta Crystallogr. D Biol. Crystallogr.* **55**, 1098–1100 (1999).
57. Heil, C. S., Rittner, A., Goebel, B., Beyer, D. & Grininger, M. Site-specific labelling of multidomain proteins by Amber Codon suppression. *Sci. Rep.* **8**, B08206 (2018).

Acknowledgements

We thank Kim Remans for helpful discussions. We are grateful to Ilka Siebels for providing Sfp and Alexander Rittner for providing holo *mm*ACP-H8. We thank Emily Hensch and Dominik Scheliu, who assisted in this project during her bachelor thesis and his master thesis, respectively. This work was supported by intramural funds of the Goethe University Frankfurt to M.G., and was associated to the LOEWE program (Landes-Offensive zur Entwicklung wissenschaftlich-ökonomischer Exzellenz) of the state of Hesse conducted within the framework of the MegaSyn Research Cluster. Open access funding provided by Projekt DEAL.

Author contributions

F.B. cloned several protein expression constructs and prepared several proteins. F.B. further established protocols, designed experiments, analysed data, prepared all figures and tables, and designed research. Y.K. cloned protein expression constructs and prepared proteins used for western blotting (except *mt*Dod constructs). Y.K. also conducted the western blots and analysed data. J.L. (under supervision of F.B.) cloned several protein expression constructs, purified *mt*Dod-PAS-Pep constructs, prepared several proteins, and analysed data. I.G. cloned *mt*Dod-PAS-Pep constructs and expressed them in *E. coli*. H.B. designed research. R.M.V. selected peptide sequences used for AB production. M.G. analysed data and designed research. F.B. and M.G. wrote the paper. Y.K., R.M.V., and H.B. edited the paper. All authors reviewed the paper.

Competing interests

F.B., H.B., I.G., and M.G. are inventors of EP patent application "Carrier Matrix Comprising Dodecin Protein", EP19220117.6 (filed on December 30th, 2019) for the use of dodecins for antibody production. The remaining co-authors have no conflicts of interest with the content of this article.

Additional information

Supplementary information is available for this paper at https://doi.org/10.1038/s41598-020-69990-0.

Correspondence and requests for materials should be addressed to M.G.

Reprints and permissions information is available at www.nature.com/reprints.

Publisher's note Springer Nature remains neutral with regard to jurisdictional claims in published maps and institutional affiliations.